CURRENT EYE RESEARCH
2018, VOL. 43, NO. 9, 1160–1168
https://doi.org/10.1080/02713683.2018.1482557

Taylor & Francis
Taylor & Francis Group

Small GTPase RIT1 in Mouse Retina; Cellular and Functional Analysis

Sajad Mir and Douglas A. Andres

Department of Molecular and Cellular Biochemistry, University of Kentucky, College of Medicine, Lexington, Kentucky, US

ABSTRACT

Purpose: Ras-like without CAAX 1 (*RIT1/*Rit) is a member of the Ras subfamily of small GTP-binding proteins with documented roles in regulating neuronal function, including contributions to neurotrophin signaling, neuronal survival, and neurogenesis. The aim of the study was to (1) examine the expression of RIT1 protein in mouse retina and retinal cell types and (2) determine whether RIT1 contributes to retinal ganglion cell (RGC) survival and synaptic stability following excitotoxic stress.

Materials and methods: Gene expression and immunohistochemical analysis were used to examine RIT1 expression in the mouse retina. Primary RGC and Müller glia cultures were used to validate novel *RIT1* lentiviral RNAi silencing reagents, and to demonstrate that RIT1 loss does not alter RGC morphology. Finally, *in vitro* glutamate exposure identified a role for RIT1 in the adaptation of RGCs to excitotoxic stress.

Results: Gene expression analysis and immunohistochemical studies in whole eyes and primary cell culture demonstrate RIT1 expression throughout the retina, including Müller glia and RGCs. While genetic RIT1 knockout (*RIT1-KO*) does not affect gross retinal anatomy, including the thickness of constituent retinal layers or RGC cell numbers, RNAi-mediated *RIT1* silencing results in increased RGC death and synaptic loss following exposure to excitotoxic stress.

Conclusions: RIT1 is widely expressed in the murine retina, including both Müller glia and RGCs. While genetic deletion of RIT1 does not result in gross retinal abnormalities, these studies identify a novel role for RIT1 in the adaptation of RGC to excitotoxic stress, with RIT1 promoting both neuronal survival and the retention of PSD-95^{+} synapses.

ARTICLE HISTORY
Received 14 December 2017
Accepted 14 May 2018

KEYWORDS
Ras GTPase; retina; Müller glia; excitotoxicity; neuronal death

Introduction

The Ras superfamily of low molecular weight GTP-binding proteins are a group of structurally related, and evolutionarily conserved proteins, which share the ability to undergo guanine nucleotide-dependent conformational change.[1] Ras family G-protein activation is under the control of guanine nucleotide exchange factors which promote nucleotide release and increase GTP-binding, which results in a conformational change within the effector (G2) domain. When GTP-bound, Ras G-proteins recruit cellular effector proteins, which in turn result in the activation of diverse cellular signaling cascades.[2] Signal transduction terminates when the hydrolysis of bound GTP returns small G-proteins to their "inactive" GDP-bound conformational state.[3] GTPase-activating proteins accelerate the intrinsic GTPase activity of Ras superfamily members and comprise a second set of regulatory factors.[4,5] Over 100 members of the Ras superfamily have been identified, including the vertebrate *RIT1* (RIT1, Rit) and *RIT2* (RIT2, Rin) proteins, which along with *Drosophila D-Ric*, comprise the Rit subfamily of GTP-binding proteins.[2]

We have a long-standing interest in understanding the physiological function of RIT1, including identified roles for RIT1 in the regulation of a variety of MAP kinase cascades, mTOR, and Akt signaling cascades.[6–10] Importantly, these studies have led to the identification of RIT1 as a central regulator of *in vivo* pro-survival signaling in response to oxidative stress,[6] in the control of neural stem cell homeostasis,[7–9] as a driver oncogene in a subset of human lung adenocarcinomas,[11] and for gain-of-function *RIT1* mutations as a cause of Noonan syndrome.[12–16]

RIT1 is widely expressed,[17,18] including within the developing and adult central nervous system and eyes.[17,19,20] In our recent characterization of *RIT1* mutations identified from Noonan's syndrome patients,[12] the introduction of gain-of-function mutations into zebrafish embryos resulted in eye abnormalities, suggesting a potential role for *RIT1* signaling in the vertebrate eye. While we have recently developed transgenic *RIT1*-KO mice to explore the physiological function of RIT1,[7,9] and RIT1 mRNA is found in the retina,[17] a detailed analysis of RIT1 protein expression has not been performed. Therefore, here we examine RIT1 expression in mouse retina utilizing a variety of molecular techniques, and demonstrate its expression in diverse retinal cell types. While genetic disruption of RIT1 expression did not result in gross retinal abnormalities, *RIT1* deficiency sensitizes primary retinal ganglion cell (RGC) cultures to excitotoxic stress, resulting in greater cell death and synaptic loss following glutamic acid exposure. These data suggest for the first time that RIT1 plays a critical role in RGC recovery from excitotoxic stress.

CONTACT Sajad Mir sajad.mir@uky.edu; Douglas A. Andres dandres@uky.edu Department of Molecular & Cellular Biochemistry, University of Kentucky College of Medicine, BBSRB 149, 741 S. Limestone Street, Lexington, KY 40536-0509

Color versions of one or more of the figures in the article can be found online at www.tandfonline.com/icey.

Materials and methods

Gene expression analysis

Total RNA from either whole eye, liver ($n = 4$), or cultured Müller glia/RGCs ($n = 6$) was prepared using the SV total RNA isolation kit as per the manufacturer's instructions (Promega-Z3101). Following isolation, RNA (100 µg) was used for cDNA synthesis (using iScript cDNA Synthesis Kit by Bio-Rad) from either whole retina or liver using *RIT1*-specific primers (see Table 1 for details). RT-PCR primers, designed to recognize murine RIT1 transcript variant 2 (exon-4 and 5) (NCBI reference Sequence: NM_001163310.1), were used to amplify cDNA for 32 cycles with the following parameters: 95°C for 30 s, 58°C for 60 s, and 72°C for 45 s, using DreamTaq Green DNA polymerase (Thermofisher Scientific) and resolved on 1–2% agarose gels. Images were captured using Gel doc (BioRad).

Tissue collection and processing

Wild-type (WT) C57BL/6J mice (Jackson Laboratories, Bar Harbor, ME, USA) and *RIT1* knockout (*RIT1*-KO) mice were used in this study. Details of the genotyping and initial characterization of *RIT1-KO* mouse have been described.[7] Maintenance of the animals adhered to institutional guidelines for the humane treatment of animals.

Animals received an overdose of Fatal-plus (150 mg/kg intraperitoneal), and were perfused with 0.98% saline, followed by 4% paraformaldehyde.[21] Eyes were removed from the skull and immediately post-fixed in 4% paraformaldehyde at 4°C for 2 days. Eyes were then washed extensively to remove excess paraformaldehyde and incubated in increasing concentrations of 10–30% sucrose solution overnight for 3 days at room temperature. Eyes were embedded in optimal cutting compound (OCT), and placed at −80°C for at least 2 days before sectioning using a cryostat.

Morphometric analysis of retina and RGC counting

A single observer performed retinal morphometric analysis from 40 µm thick sections from WT and RIT1-KO mice (n = 3 per genotype). Mean retinal thickness was calculated from measurements of three consecutive retinal sections for each eye sample taken at two locations: the central (within one optic nerve diameter from the optic nerve margin) and peripheral retina (within one 40× field from the anterior margin, Ora serrata).[22,23] The parameters included thickness of the combined nerve fiber and ganglion layers (NFL/GCL); the inner plexiform layer (IPL), inner nuclear layer (INL), outer plexiform layer (OPL), outer nuclear layer (ONL), photoreceptor (PR)layer; and the retinal pigment epithelium (RPE). For RGC counting analysis, WT and RIT1-KO mice retinal sections were stained with the RGC marker Brn3a and Z-stack images (with each stack at least 3 µm), and were captured using laser scanning confocal microscope (Nikon A1 with a motorized stage). Best-fit Z-stack images were stitched together and converted to 8-bit depth images with grey scale prior to analysis using the cell-counting tool from Image-J as described.[24]

Immunofluorescence

Immunofluorescence or immunocytochemistry was performed using our previously published methods.[8,9,21] Briefly, mice were anesthetized with sodium pentobarbital (65 mg/kg, i.p.), transcardially perfused with 0.98% saline, followed by fixation with 4% paraformaldehyde. Eye balls (n = 8) were removed from the skull, subject to post-fixation (2–3 days, see above for details). Eye balls were embedded in OCT and snap frozen. Blocks were stored at −80°C for at least 2 days before coronal sections (40 µm), were cut using a cryostat and mounted on Superfrost plus slides (Fisher). Antigen retrieval was performed in citrate buffer (pH 6.2, 85°C, three runs 30 s each). PSD95 antigen retrieval was done with a solution with 0.25% trypsin containing 2N HCl at room temperature for 10 min. Serial sections (40 µm, n = 12/eye) were extensively washed with PBS and incubated in blocking and permeabilizing buffer [1% serum (matching the secondary antibody host), 1% Triton X-100 in 1× PBS)] for 10 min at RT followed by extensive washing (4× PBS). Primary antibodies were diluted in blocking buffer (0.01 M PBS pH 7.2 containing 1% serum, 0.05% Tween 20, and 0.1% Triton X-100) and applied to the sections O/N (4°C). Antibodies used were mouse anti PSD95,

Table 1. List of RT-PCR primers, *RIT1* RNAi target sequence, and commercial antibodies used in this investigation.

RIT1 (mouse NM_009069) primer pair 1(209bp)	Forward 5′-GGTCTGTGGTGTCTCTGTCC-3′ Reverse 5′-CTTATCCAGGATCCAACGTG-3′
RIT1 (mouse NM_009069) primer pair 2(137bp)	Forward 5′-TGGGACCATTGCTGGATGAC-3′ Reverse 5′-GCCAGGGTAACCTCAACCTC-3′
RIT1 (mouse NM_009069) Pri ShRNA target sequence	TGCTGTTGACAGTGAGCGACACGAAGTTCGGGAGTTTAAATAGTGA AGCCACAGATGTATTTAAACTCCCGAACTTCGTGGTGCCTACTGCCTCGGA
Rit1 mouse genotyping primers sets	Wild Type Reaction: 250bp product Forward 5′-GTGAAGGGGCGAGGATGTAGG-3′ Reverse 5′-GTATTCCCGGGAGAGTGCTG-3′ Mutant Type Reaction: 347bp product Forward 5′-ACCCGGGAGAGTGCTGAAGAGC-3′ Reverse 5′-GGTCATGGTCTTCTGGGAATCG-3′
RIT1 (mouse monoclonal) (SC-58473)	Santa Cruz Biotechnology (1:200)
Brn3a (goat polyclonal)	Santa Cruz Biotechnology (1:200)
Vimentin (mouse monoclonal) (40-E-C-S)	DSHB (1:200)
CRALBP (mouse monoclonal) (MA1-813)	Thermofisher Scientific (1:350)
PSD95 (mouse monoclonal)	Neuromab (1:400)
Anti mouse IgG Alexa Flour 488	Invitrogen (1:1000)
Anti goat IgG Alexa Flour 488	Invitrogen (1:1000)
Anti mouse IgG Alexa Flour 594	Cell signaling technology (1:1000)

mouse anti-RIT1, goat anti-Brm3a, rabbit anti-vimentin, and mouse anti-CRALBP (see Table 1 for details). On the following day, sections were washed four times with 1× PBS, and secondary antibody (conjugated with either Alexa 488, Alexa 568, Alexa 594, or PE) diluted in blocking buffer, was applied for 2 h in the dark. Sections were then washed with 1× PBS, air dried, and cover slipped in slow fade gold containing 4',6-diamidino-2-phenylindole (DAPI). For immunocytochemistry, cells were fixed in 4% paraformaldehyde for 15 min at room temperature, permeablized, and blocked using similar solutions and antibody dilutions as described above for tissue sections. Representative images were captured using a Nikon CKX31 A1 confocal microscope or Nikon C2 confocal microscope using the NIS-Elements software package (University of Kentucky License).

Co-localization analysis via laser scanning confocal microscopy

Images were collected using a Nikon A1 confocal microscope in batches (at least 3–5 slides/mouse; a minimum of 18 retina sections/four mice/genotype) with pinhole adjusted to 1.2 airy units (A.U.). Immunolabeling was assessed in a minimum of 18 retina sections from four animals. To assess RIT1 cellular co-localization, surface intensity of the image was determined using resonance mode and the Z-stack was fixed. Scanning was performed at 1024 pixels at 16× speed. The coefficient of co-localization was determined by setting a region of interest (ROI) on the Z-stack in the maximum intensity mode. On average, 4–6 ROIs were used to generate coefficient of correlation (at least three slides/six sections per slide, $n = 4$). Final images were prepared using NIS Elements software (licensed to the University of Kentucky).

Immunoblotting

Tissues/cells were homogenized using a Next Advance Bullet Blender at 4°C in lysis buffer (20 mM Tris·HCl pH 7.5, 250 mM NaCl, 10 mM $MgCl_2$, 1% Triton X-100, 1 mM Na_3VO_4, 50 mM β-glycerophosphate, 1× protease inhibitor cocktail). Cleared whole cell lysates (14,000 rpm for 10 min) were generated, and protein concentration determined by the Bradford method. Lysates were resolved by 12% SDS-PAGE, transferred to nitrocellulose membranes O/N (12 h, 0.08 mA), and subjected to Western blotting with the indicated antibodies (see Table 1) by chemiluminescence (HyGlo, Denville Scientific) using a ChemiDoc MP with Image Lab software (Bio-Rad)).

RIT1-specific RNA*i* and transduction

Lentiviral vector pZIP-mCMV-Zs Green containing the *RIT1* pri-shRNA sequence (TGCTGTTGACAGTGAGCGACACG AAGTTCGGGAGTTTAAATAGTGAAGCCACAGATGTAT TTAAACTCCCGAACTTCGTGGTGCCTACTGCCTCGGA) was purchased (TransOMIC Technologies).[9] Lentivirus was generated in 293LTV cells using the packaging vectors PsPAX2 and pMD2.G (Univ. Kentucky Genetic Technology Core). Briefly, cultured primary Müller glia or RGCs were allowed to grow to 15 DIV (days *in vitro*) before the experiments. Polybrene (1 µl, 10 mg/mL) (Santa Cruz Biotechnology) was added to cells for 10 min at 37°C followed by repeated washes in 1× DPBS. New growth medium was premixed with 3MOIs of either non-targeting control or anti-*RIT1* targeting lentivirus and placed on cells for 4–12 h at 37°C. Transduction medium was replaced and cells allowed to recover for 48–72 h before analysis.

Isolation of primary Müller glia

Müller glia were isolated from 2–5-day-old pups and cultured as described,[25] with minor modifications. Briefly, eyes were removed and placed in 1× HBSS (Hanks balanced salt solution), rinsed in phosphate-buffered saline (PBS), and incubated in 2 mL of retinal digestion buffer containing trypsin (.25%), EDTA (28 mM), and collagenase (2 mg/mL). Retinas were dissected and dissociated to achieve a single cell suspension. The retinal suspension was seeded onto poly-D-lysine-coated tissue culture plates in DMEM high glucose supplemented with 5% fetal bovine serum (FBS) and antibiotic solution (1×). After 4–7 days in culture, the monolayer was washed vigorously (to remove non-adherent cells most of which are loosely adherent microglia and macrophages) with medium until only strongly adherent cells remained. Cells were used at passage 4–5. The percentage of Müller glia in this cell population was assessed by immunohistochemistry using antibodies against the known Müller cell markers vimentin and CRALBP.[26] This analysis failed to detect non-vimentin$^+$/CRALBP$^+$ cells, indicating that the resulting cultures were highly enriched.

Isolation of primary retinal ganglion cells (RGCs)

Primary RGCs were isolated from the retinas of 7-day mouse pups using published immune panning methods.[27] Briefly, eye balls were collected in 1× HBSS and subjected to enzyme digestion in retinal digestion buffer for 25 min as described above for Müller glia. The resulting single cell suspension was incubated with anti-F4/80 antibody (1 µg/mL in PBS, pH 7.4) for 30 min at RT to deplete the macrophage and microglia, prior to being transferred to rabbit anti-IgG-pretreated plastic plates. Non-adherent cells were collected after 30 min and incubated in anti-Thy1.1-coated plates for 1 h. Adherent RGCs were collected, washed with PBS (three times), plated on poly-D-lysine hydrobromide (PDL)-coated coverslips, and allowed to recover for 12 days in medium containing Neurobasal/DMEM (1:1) supplemented with 2% B27 supplement, with medium changes in every 3–5 days. Brn3a immunocytochemistry was used to assess panning efficiency, and the resulting cultures were regularly comprised of >90% RGCs (Brn3a$^+$ cells).

PSD-95 synaptic density assessment

Immunofluorescence was used to examine the impact of RIT1 deficiency on the *in vivo* and *in vitro* density of PSD95$^+$ synapses. Images from PSD95 stained sections (3–5 sections, 40 µm each) were obtained from WT and RIT1-KO mice ($n = 3$/genotype). Batches of images (2–4) from the central and peripheral retina were analyzed using Image-J and pixel density measurements performed on 8-bit greyscale images. For analysis of cultured primary RGCs, PSD95 density analysis was performed using Neuron Studio software (Computational Neurobiology and Imaging Center, Mount Sinai School of Medicine New York, NY). PSD95$^+$ synapses were identified as greater than or equal to twice the signal value when compared to a null background. Spine attachments were constructed along apical dendrites and density was estimated from 10 μm segments as per our published methods.[21]

RGC morphology tracing

Cultured RGCs (DIV 12) were grown on glass coverslips in DMEM/Neurobasal media (1:1) and subject to lentiviral infection as described above. Coverslips were fixed (72 h post-infection) in 4% paraformaldehyde containing sucrose (15%) for 35 min at RT, washed with PBS (pH 7.1), and ZS-Green+ RGCs analyzed by confocal microscopy. Axonal and dendritic lengths were measured (5–10 RGCs per group) using Neuron Studio software.

RGC excitotoxicity-mediated cell death and synaptic loss

Cultured RGCs (~18 DIV) were treated with polybrene (1 µl, 10 mg/mL, Santa Cruz Biotechnology), prior to the addition of either non-targeting control RNA*i* or *RIT1* and targeting RNA*i* (3MOIs); the medium was replaced following a 6–8 h transduction period, and RGCs were allowed to recover for 24–48 h. Infected RGCs were either treated with 100 µM glutamic acid or PBS, and cell viability was monitored using a MTT assay (Sigma), and optical density recorded using a plate reader (Molecular Devices, Sunnyvale USA) at 570 nm. Laser scanning confocal microscope (Nikon A1R) at 40× magnification too permit the resolution needed to evaluate individual PSD95$^+$ spines, and neuron studio software was used to calculate spine density.[21,28]

Statistical analysis

Data analysis involved either nonparametric one tailed *t*-test or one-way ANOVA using GraphPad Prism (La Jolla, CA). Tukey Kramer multiple comparison tests was the *post hoc* test with group numbers >2. A *p*-value of <0.05 was considered significant in all forms of analysis.

Results

RIT1 expression in the murine eye

RT-PCR was used to analyze expression of *RIT1* (NM_009069, transcript variant 2) in the mouse eye, using two different primer pairs (products 209 and 139 bp), targeting two distinct exons of the predominant expressed transcript (encoding full-length murine RIT1). With mouse liver serving as a positive control,[29] endogenous RIT1 mRNA expression was seen in the eye (Figure 1), in agreement with earlier Northern blot studies.[17,30]

To extend this analysis, immunoblotting confirmed RIT1 protein expression in whole eye lysates (Figure 2A and B). As RIT1 is expressed in diverse cell types,[31] we next used confocal laser-scanning microscopy to examine endogenous RIT1 protein expression within the retina (Figure 2C), demonstrating broad RIT1 expression. Immunofluorescence failed to detect expression in the retina from RIT1-KO mice, providing a crucial specificity control (Figure 2C). Signal intensity measurements (data not shown) indicate that RIT1 is expressed most abundantly in the inner GCL, plexiform layers (IPL and OPL), and in RPE (Figure 2C). Gross anatomical observation showed no gross abnormality of retinal structure in RIT1-KO mice when compared to the WT mice. Measurement of the thickness of individual retinal layers (GCL. IPL, OPL, INL ONL, PR, and RPE) from both the central and peripheral retina (Figure 2C) were similar in WT and RIT1-KO mice ($p > 0.05$) (Figure 2D). Taken together, these data suggest that RIT1 is widely expressed within the retina, but is not required for eye formation.

RIT1 expression in Müller glia and retinal ganglion cells

To extend analysis of RIT1 expression to additional retinal cell types, we next analyzed RIT1 expression in primary RGCs and Müller glia cultures. Confocal laser scanning Z-stacking analysis of RIT1 and the Müller glia marker CRALBP[26,32] in retina finds RIT1 expression in CRALBP$^+$ Müller glia (Figure 3A, Pearson coefficient = 0.5). As seen in Figure 3B, infection of cultured mouse Müller glia with an engineered lentivirus co-expressing Zs-green (coral green protein, permitting visual detection of infected cells) and a RIT1-specific RNA*i* target sequence resulted in efficient reduction of

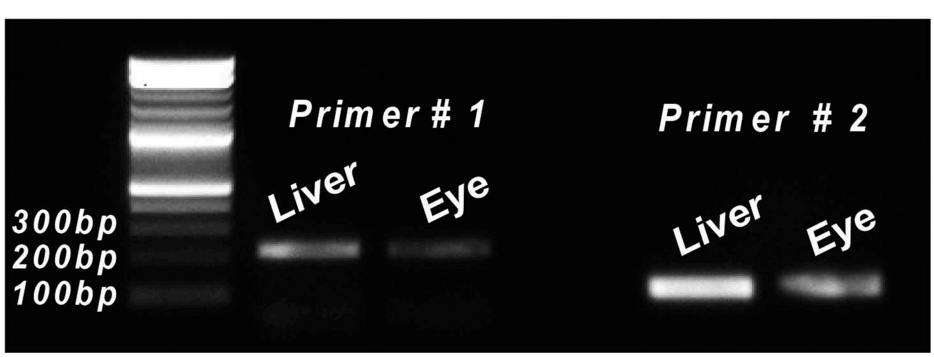

Figure 1. *RIT1* expression in the eye. RT-PCR analysis (n = 4) demonstrates RIT1 expression in eye. Total liver mRNA served as a positive control.31 The primer sets detect functional slice variants.

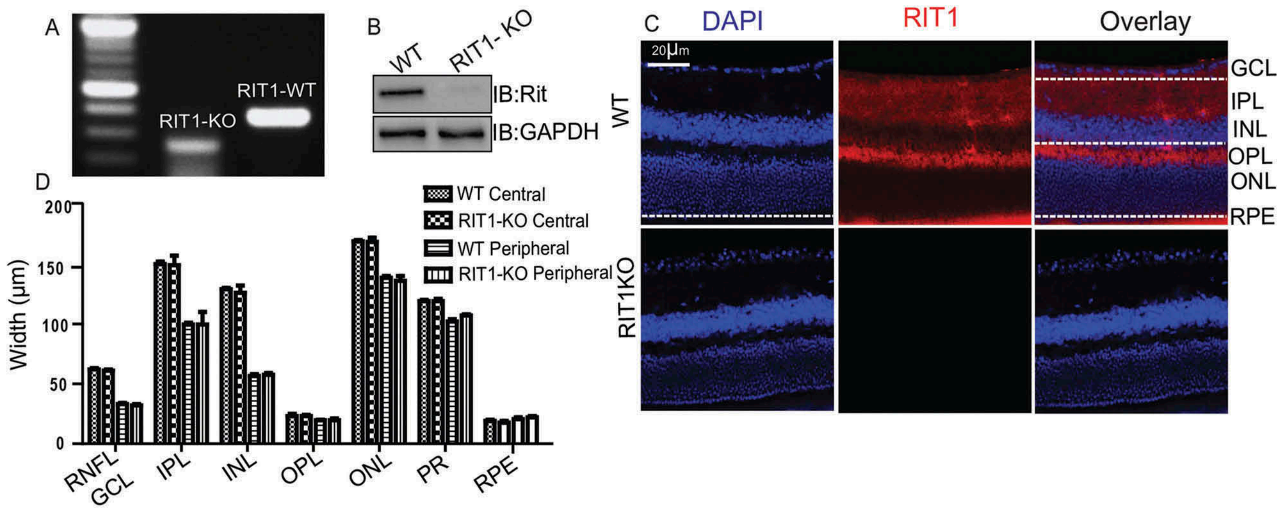

Figure 2. Retinal RIT1 expression. (A) Genotyping PCR from wild-type (WT) and *RIT1-KO* littermates. (B) Western analysis of endogenous RIT1 protein expression. GAPDH served as normalization control. (C) Representative confocal micrographs of RIT1 (red) and DAPI counterstained (nuclei, blue) expression in coronal sections of naïve WT and RIT1-KO retina reveals strong RIT1 labeling in the IPL, OPL, and RPE of WT mice. Scale bar 20 µm. (D) Central and peripheral retinal layer thickness in WT and RIT1 KO mice (three independent measurements from $n = 3$/genotype). Note that no significant difference is detected ($p > 0.05$). RPE: retinal pigmented epithelium; ONL: outer nuclear layer: OPL: outer plexiform layer; INL: inner nuclear layer; IPL: inner plexiform layer; and GCL: ganglion cell layer.

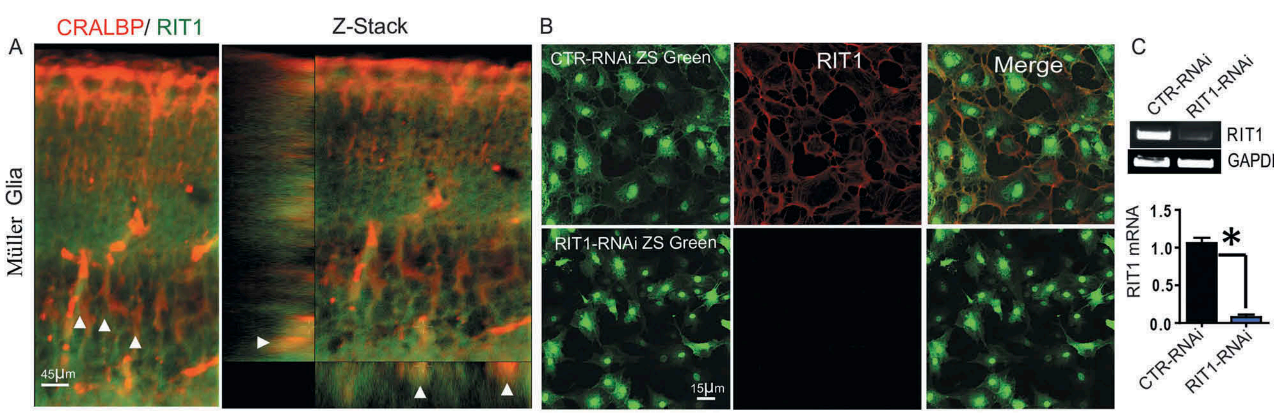

Figure 3. (A) *In vivo* immunofluorescence analysis of RIT1 in Müller glia. Representative confocal micrographs of RIT1 (green) and the Müller glia cell-specific marker CRALBP (red) from naïve WT retina. Arrowheads (white) indicate $RIT1^+$/$CRALBP^+$ Müller glia (co-localization in Z-stack with a coefficient of correlation $R = 0.5$; yellow). Scale bar 45 µm. (B) Representative confocal images of lentiviral RNAi infected (ZS-$Green^+$) Müller glia (48–72 h) stained for RIT1 (red). Scale bar 20 µm. (C) Lentiviral RNAi-dependent RIT1 silencing in Müller glia (*$p < 0.01$, $n = 3$).

endogenous RIT1 detected by immunocytochemistry. RT-PCR analysis of endogenous RIT1 mRNA found efficient (~95%) silencing in Müller glia (Figure 3C). Using an identical experimental strategy, RIT1 co-localized *in vivo* with the RGC marker Brn3a[33] (Figure 4A, Pearson coefficient = 0.6), and both endogenous RIT1 protein (Figure 4B) and mRNA (Figure. 4C) were reduced following RNAi-mediated gene silencing in primary RGCs (~95%). As earlier studies have identified a role for RIT1 in the regulation of neuronal morphogenesis,[19] we quantified the effect of RIT1 silencing on neuronal polarity and axonal growth. RIT1 deficiency had no effect on the length of axons or dendrites in cultured RGCs (Figure 4D). Taken together, these data demonstrate that both Müller glia and RGCs express RIT1, but does RIT1 not play a critical role in determining RGC morphology.

RIT1 loss sensitizes RGCs to excitotoxic cell death and synaptic loss

We have previously shown that RIT1 contributes to the regulation of neuronal survival[7] and controls an evolutionarily conserved survival mechanism for cells responding to stress,[6] but how RIT1 may affect RGC function is unknown. Analysis of total RGC numbers from the inferior, nasal, superior, and temporal quadrants of WT and KO retinas did not detect significant alterations resulting from RIT1 ablation ($p > 0.05$) (Figure 5A). Co-localization analysis in the apical dendrites of cultured RGCs found RIT1 to co-localize with the synaptic scaffolding protein PSD95, suggesting that RIT1 may contribute to synaptic regulation[34,35] (Figure 5B, Pearson coefficient = 0.7). However, *in vivo* immunostaining of the retina IPL layer from WT and RIT1-KO mice found no significant alterations in PSD95 density

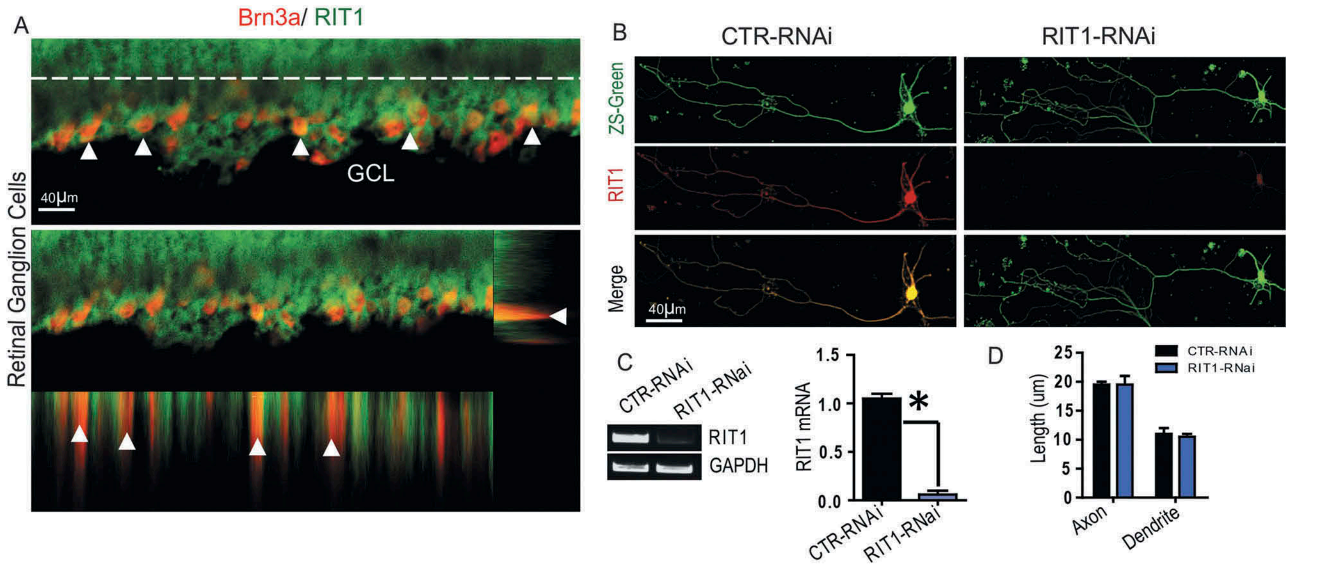

Figure 4. *In vivo* immunohistochemical analysis of RIT1 in RGCs. (A) representative Z-stacks from confocal laser scanning micrographs of the RGC layer of retina sections from naïve WT retina immunolabeled for RIT1 (green), and the RGC cell-type specific marker Brn3a (red). Arrowheads (white) indicate $RIT1^+$/$Brn3a^+$ RGCs (coefficient of co-localization $R = 0.6$). Scale bar 40 µm. (B) Representative confocal images of lentiviral RNAi infected ($ZS\text{-}Green^+$) RGCs (DIV 12) stained for RIT1 (red) at 72 h post-infection. Scale bar 100 µm. (C) Lentiviral RNAi-dependent RIT1 silencing in primary RGCs (*$p < 0.01$, $n = 3$). (D) The RIT1 silenced RGCs or non-targeted RGCs (10–15 cells/treatment) were subject to axon and dendrite tracing and average length. *$p > 0.05$ One way ANOVA ($n = 3$).

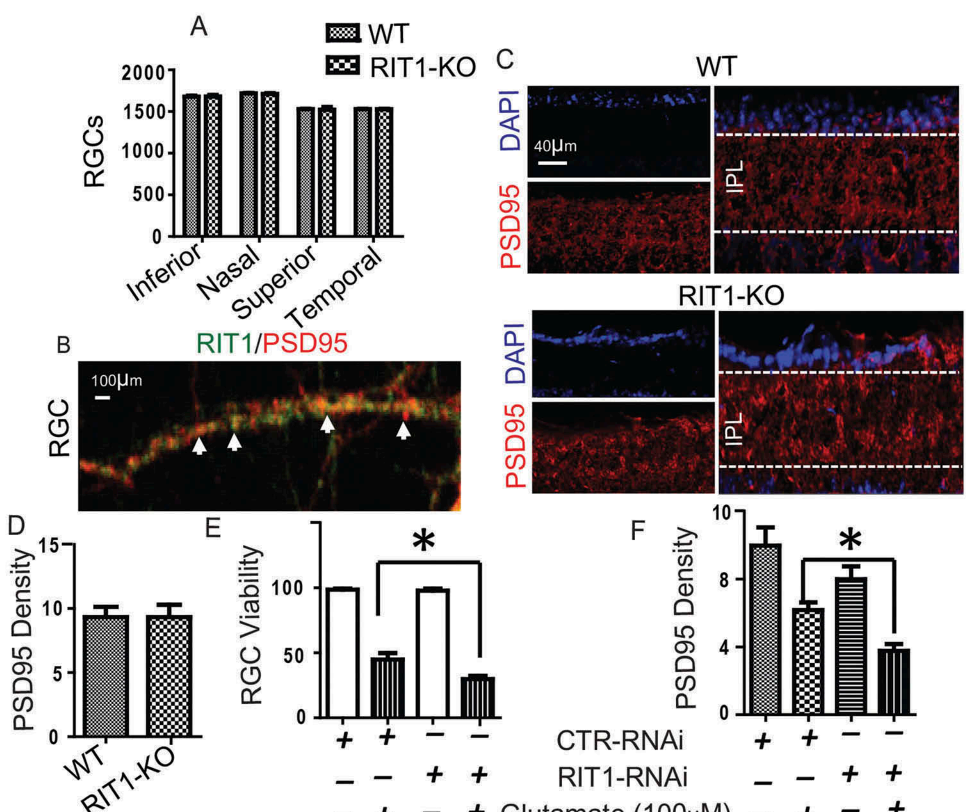

Figure 5. RIT1 loss sensitizes RGCs to excitotoxic stress. (A) Quantification of RGCs in all four quadrants (inferior, nasal, superior, and temporal) of flat mount sections from WT and RIT1-KO mice ($n = 3$/genotype). (B) Immunocytochemical analysis of RIT1 (green) and PSD95 (red) show co-localization in mouse RGCs ($n = 15$) (arrows depict co-localization $R = 0.7$ in apical dendrites). (C) Representative confocal images of PSD95 (red) and DAPI (nuclei, blue) from the retinal inner plexiform layer (IPL) of WT and RIT1-KO mice. Scale bar is 40 µm. (D) Quantification of $PSD95^+$ density in WT and RIT1-KO mice ($p > 0.05$, $n = 3$; three sections/mouse). (E) Cell viability of RGCs measure by MTT assay at 72 h following infection with either control (CTR) or RIT1 RNAi lentivirus, at 6 h after exposure to glutamate (100 µM). *$p < 0.01$, one way ANOVA ($n = 6$). (F) Density of RGC $PSD95^+$ synapses 72 h following infection with either control (CTR) or RIT1 RNAi lentivirus, was determined 6 h after exposure to glutamate (100 µM). *$p < 0.01$, one way ANOVA ($n = 10$/group).

($p > 0.05$) (Figure 5C and D). Taken together, these data indicate that genetic ablation of RIT loss does not affect either gross RGC numbers or PSD95$^+$ synapses *in vivo*.

We have shown that RIT1 deficiency alters immature hippocampal neurons in response to brain injury,[7] and that activation of RIT1 promotes hippocampal neuron survival in response to oxidative stress.[36] However, whether RIT1 contributes to the regulation of RGC survival or synaptic retention in response to cellular stress is unknown. In keeping with a central role for RIT1 in the response of RGCs to excitotoxic insult, RNAi-mediated RIT1 silencing resulted in a significant increase in RGC loss ($p < 0.01$) following glutamic acid challenge (100 µM, 5 h) (Figure 5E, CTR RNAi/glutamate = 100 ± 3%; CTR RNAi/glutamate = 47 ± 8%; RIT1 RNAi/glutamate = 100% ± 4%; RIT1 RNAi/glutamate = 28 ± 4%). Furthermore, RIT1 silencing has found to enhance the loss of PSD95$^+$ synapses following glutamate challenge (Figure 5F, $p < 0.01$). These results show that RIT1 might be necessary for RGC survival and synaptic stability during excitotoxicity.

Discussion

Using a collection of molecular and genetic tools, here we demonstrate that the RIT1 GTPase is widely expressed across the retina, including within both RGCs and Müller glia. In keeping with earlier studies defining a role for RIT1 signaling in neuronal survival,[6,7] we find that RIT1 deficiency markedly enhances the vulnerability of RGC neurons and the loss of PSD95$^+$ synapses in response to excitotoxic insult. As excitotoxicity is a prominent contributor to retinal degeneration during glaucoma, age-related macular degeneration, and retinal injury, these data suggest that RIT1 might contribute to RGC function in these disorders.

In agreement with earlier studies,[17] RT-PCR analysis finds RIT1 expression within the murine eye. Confocal microscopy reveals that although widely expressed in retina, RIT1 protein displays some variation between constituent retinal layers. Importantly, examination of WT and RIT1-KO mice show similar widths of all the constituent layers, including both the central and peripheral retina. At the cellular level, RNAi-mediated RIT1 silencing methods confirmed RIT1 expression in retinal Müller glia and RGCs.

Loss of RGCs is a leading causes of vision loss,[37–39] and can arise from diverse causes ranging from genetic lesions to traumatic visual injury.[40–47] Although the molecular mechanisms of vision loss are under intense investigation, visual disorders can result from dysfunction within evolutionary conserved neuronal survival signaling pathways. Our findings demonstrate that RIT1 is not essential for eye formation. Genetic ablation of RIT1 neither promotes gross abnormalities in retinal structure nor affects RGC numbers or expression of the postsynaptic density protein PSD95. Furthermore, *in vitro* studies suggest that RIT1 does not play a critical role in the regulation of RGC morphology, as RIT1 silencing does not affect axonal or dendritic length. However, upon excitotoxic challenge, RIT1 loss impairs RGC survival. These findings are consistent with our previous reports in which mouse embryonic fibroblasts derived from *RIT1-KO* mice display increased vulnerability to free radical stress.[48] We have also reported that neuronal expression of a constitutively active *RIT1* mutant in postnatal neurons provides p38 MAPK-dependent protection from cell death.[36] Notably, newborn neurons in *RIT1-KO* mice have been found to be especially vulnerable following brain injury,[7] which also points to a critical role for RIT1 in neuronal survival.

In summary, previous studies have identified roles for RIT1 in diverse biological processes ranging from cell survival, to neurotrophin signaling and neurogenesis. With the knowledge that diverse retinal cell types express RIT1, and that RIT1 functions as an important regulator of RGC survival in response to excitotoxic stress, this study introduces a new regulatory G-protein to retina biology. In future, it will be important to characterize the molecular mechanism of RIT1-dependent signaling to RGC recovery following excitotoxic challenge.

Acknowledgments

We wish to thank Dr. Michael Mendenhall for generation of recombinant lentiviruses. The authors acknowledge the use of facilities in the University of Kentucky, Center for Molecular Medicine Genetic Technologies Core, supported by NIH Grant P30GM110787.

Declaration of interest

The authors report no conflicts of interest. The authors alone are responsible for the content and writing of the article.

Funding

This work was supported in part by National Institutes of Health Grant [R01 NS102196] (DAA), the Kentucky Spinal Cord and Head Injury Research Trust (Grants 12-1A and 16-1) (DAA), a grant from the Kentucky Lung Cancer Research Grant (DAA) [P-02 414], and National Institute of Neurological Disorders and Stroke [NS102196]. The funders had no role in study design, data collection and analysis, or preparation of the manuscript.

Note on contributors

S. M designed the research; S. M, performed research; S. M. analyzed data; S. M and D. A. A wrote the article.

References

1. Colicelli J. Human RAS superfamily proteins and related GTPases. Sci STKE. 2004;250:Re13.
2. Shi GX, Cai W, Andres DA. Rit subfamily small GTPases: regulators in neuronal differentiation and survival. Cell Signal. 2013;25(10):2060–68. doi:10.1016/j.cellsig.2013.06.002.
3. Hoshino M, Yoshimori T, Nakamura S. Small GTPase proteins Rin and Rit Bind to PAR6 GTP-dependently and regulate cell transformation. J Biol Chem. 2005;280(24):22868–74. doi:10.1074/jbc.M411592200.
4. Wennerberg K, Rossman KL, Der CJ. The Ras superfamily at a glance. J Cell Sci. 2005;118(Pt 5):843–46. doi:10.1242/jcs.01660.
5. Rojas AM, Fuentes G, Rausell A, Valencia A. The Ras protein superfamily: evolutionary tree and role of conserved amino acids. J Cell Biol. 2012;196(2):189–201. doi:10.1083/jcb.201103008.
6. Cai W, Andres DA. mTORC2 is required for rit-mediated oxidative stress resistance. PLoS One. 2014;9(12):e115602. doi:10.1371/journal.pone.0115602.
7. Cai W, Carlson SW, Brelsfoard JM, Mannon CE, Moncman CL, Saatman KE, Andres DA. Rit GTPase signaling promotes immature

hippocampal neuronal survival. J Neurosci. 2012;32(29):9887–97. doi:10.1523/JNEUROSCI.0375-12.2012.
8. Mir S, Cai W, Andres DA. RIT1 GTPase regulates Sox2 transcriptional activity and hippocampal neurogenesis. J Biol Chem. 2016;292:2054–64.
9. Mir S, Cai W, Carlson SW, Saatman KE, Andres DA. IGF-1 mediated neurogenesis involves a novel RIT1/Akt/Sox2 cascade. Sci Rep. 2017;7(1):3283. doi:10.1038/s41598-017-03641-9.
10. Shi GX, Cai W, Andres DA. Rit-mediated stress resistance involves a p38-mitogen- and stress-activated protein kinase 1 (MSK1)-dependent cAMP response element-binding protein (CREB) activation cascade. J Biol Chem. 2012;287(47):39859–68. doi:10.1074/jbc.M112.384248.
11. Berger AH, Imielinski M, Duke F, Wala J, Kaplan N, Shi GX, Andres DA, Meyerson M. Oncogenic RIT1 mutations in lung adenocarcinoma. Oncogene. 2014;33(35):4418–23. doi:10.1038/onc.2013.581.
12. Koenighofer M, Hung CY, McCauley JL, Dallman J, Back EJ, Mihalek I, Gripp KW, Sol-Church K, Rusconi P, Zhang Z, et al. Mutations in RIT1 cause Noonan syndrome – additional functional evidence and expanding the clinical phenotype. Clin Genet. 2016;89(3):359–66. doi:10.1111/cge.12608.
13. Kouz K, Lissewski C. Genotype and phenotype in patients with Noonan syndrome and a RIT1 mutation. Genetics in Medicine. 2016;18(12):1226–34.
14. Aoki Y, Niihori T, Banjo T, Okamoto N, Mizuno S, Kurosawa K, Ogata T, Takada F, Yano M, Ando T, et al. Gain-of-function mutations in RIT1 cause Noonan syndrome, a RAS/MAPK pathway syndrome. Am J Hum Genet. 2013;93(1):173–80. doi:10.1016/j.ajhg.2013.05.021.
15. Arroyo-Carrera I, Solo De Zaldivar-Tristancho M, Martin-Fernandez R, Vera-Torres M, Gonzalez De Buitrago-Amigo JF, Botet-Rodriguez J. RIT1: a novel gene associated with Noonan syndrome. Rev Neurol. 2016;63:358–62.
16. Yaoita M, Niihori T, Mizuno S, Okamoto N, Hayashi S, Watanabe A, Yokozawa M, Suzumura H, Nakahara A, Nakano Y, et al. Spectrum of mutations and genotype-phenotype analysis in Noonan syndrome patients with RIT1 mutations. Hum Genet. 2016;135(2):209–22.
17. Lee CH, Della NG, Chew CE, Zack DJ. Rin, a neuron-specific and calmodulin-binding small G-protein, and Rit define a novel subfamily of ras proteins. J Neurosci. 1996;16(21):6784–94. doi:10.1523/JNEUROSCI.16-21-06784.1996.
18. Spencer ML, Shao H, Tucker HM, Andres DA. Nerve growth factor-dependent activation of the small GTPase Rin. J Biol Chem. 2002;277(20):17605–15. doi:10.1074/jbc.M111400200.
19. Lein PJ, Guo X, Shi GX, Moholt-Siebert M, Bruun D, Andres DA. The novel GTPase Rit differentially regulates axonal and dendritic growth. J Neurosci. 2007;27(17):4725–36. doi:10.1523/JNEUROSCI.5633-06.2007.
20. Wes PD, Yu M, Montell C. RIC, a calmodulin-binding Ras-like GTPase. Embo J. 1996;15:5839–48.
21. Mir S, Sen T, Sen N. Cytokine-induced GAPDH sulfhydration affects PSD95 degradation and memory. Mol Cell. 2014;56(6):786–95. doi:10.1016/j.molcel.2014.10.019.
22. Ding K, Scortegagna M, Seaman R, Birch DG, Garcia JA. Retinal disease in mice lacking hypoxia-inducible transcription factor-2alpha. Invest Ophthalmol Vis Sci. 2005;46(3):1010–16. doi:10.1167/iovs.04-0788.
23. Sandbach JM, Coscun PE, Grossniklaus HE, Kokoszka JE, Newman NJ, Wallace DC. Ocular pathology in mitochondrial superoxide dismutase (Sod2)-deficient mice. Invest Ophthalmol Vis Sci. 2001;42:2173–78.
24. Danias J, Shen F, Goldblum D, Chen B, Ramos-Esteban J, Podos SM, Mittag T. Cytoarchitecture of the retinal ganglion cells in the rat. Invest Ophthalmol Vis Sci. 2002;43:587–94.
25. Takeda M, Takamiya A, Jiao JW, Cho KS, Trevino SG, Matsuda T, Chen DF. Alpha-aminoadipate induces progenitor cell properties of Muller glia in adult mice. Invest Ophthalmol Vis Sci. 2008;49(3):1142–50. doi:10.1167/iovs.07-0434.
26. Grosche A, Hauser A, Lepper MF, Mayo R, Von Toerne C. The proteome of native adult muller glial cells from murine retina. Molecular Cellular Proteomics. 2016;15(2):462–80.
27. Winzeler A, Wang JT. Purification and culture of retinal ganglion cells from rodents. Cold Spring Harb Protoc. 2013;2013:643–52.
28. Rodriguez A, Ehlenberger DB, Dickstein DL, Hof PR, Wearne SL. Automated three-dimensional detection and shape classification of dendritic spines from fluorescence microscopy images. PLoS One. 2008;3(4):e1997. doi:10.1371/journal.pone.0001997.
29. Li JT, Liu W, Kuang ZH, Chen HK, Li DJ, Feng QS, Liu QC, Hu B. Amplification of RIT1 in hepatocellular carcinoma and its clinical significance. Ai Zheng. 2003;22:695–99.
30. Spencer ML, Shao H, Andres DA. Induction of neurite extension and survival in pheochromocytoma cells by the Rit GTPase. J Biol Chem. 2002;277(23):20160–68. doi:10.1074/jbc.M201092200.
31. Liu GY. cDNA cloning, sequence identification and tissue expression distribution of three novel porcine genes: UCHL3, RIT1 and CCND3. Mol Biol Rep. 2009;36(3):521–28. doi:10.1007/s11033-008-9209-4.
32. Hippert C, Graca AB, Barber AC, West EL, Smith AJ, Ali RR, Pearson RA. Muller glia activation in response to inherited retinal degeneration is highly varied and disease-specific. PLoS One. 2015;10(3):e0120415. doi:10.1371/journal.pone.0120415.
33. Sajgo S, Ghinia MG, Brooks M, Kretschmer F, Chuang K, Hiriyanna S, Wu Z, Popescu O, Badea TC. Molecular codes for cell type specification in Brn3 retinal ganglion cells. Proc Natl Acad Sci U S A. 2017;114(20):E3974–e3983. doi:10.1073/pnas.1618551114.
34. Kerschensteiner D, Morgan JL, Parker ED, Lewis RM, Wong RO. Neurotransmission selectively regulates synapse formation in parallel circuits in vivo. Nature. 2009;460(7258):1016–20. doi:10.1038/nature08236.
35. Chen YP, Chiao CC. Spatial distribution of excitatory synapses on the dendrites of ganglion cells in the mouse retina. PLoS One. 2014;9(1):e86159. doi:10.1371/journal.pone.0086159.
36. Cai W, Rudolph JL, Sengoku T, Andres DA. Rit GTPase regulates a p38 MAPK-dependent neuronal survival pathway. Neurosci Lett. 2012;531(2):125–30. doi:10.1016/j.neulet.2012.10.036.
37. Akaiwa K, Namekata K, Azuchi Y, Guo X, Kimura A, Harada C, Mitamura Y, Harada T. Edaravone suppresses retinal ganglion cell death in a mouse model of normal tension glaucoma. Cell Death and Disease. 2017;8(7):e2934.
38. Krishnan A, Fei F, Jones A, Busto P. Overexpression of soluble fas ligand following adeno-associated virus gene therapy prevents retinal ganglion cell death in chronic and acute murine models of glaucoma. Journal of Immunology. 2016;197(12):4626–38.
39. Li LU, Zhao Y, Zhang H. P16INK4a upregulation mediated by TBK1 induces retinal ganglion cell senescence in ischemic injury. Cell Death Dis. 2017;8(4):e2752. doi:10.1038/cddis.2017.169.
40. Baltmr A, Duggan J, Nizari S, Salt TE, Cordeiro MF. Neuroprotection in glaucoma - is there a future role? Exp Eye Res. 2010;91(5):554–66. doi:10.1016/j.exer.2010.08.009.
41. Vidal-Sanz M, Salinas-Navarro M, Nadal-Nicolas FM, Alarcon-Martinez L, Valiente-Soriano FJ, De Imperial JM, Aviles-Trigueros M, Agudo-Barriuso M, Villegas-Perez MP. Understanding glaucomatous damage: anatomical and functional data from ocular hypertensive rodent retinas. Prog Retin Eye Res. 2012;31(1):1–27. doi:10.1016/j.preteyeres.2011.08.001.
42. Watanabe M, Sawai H, Fukuda Y. Survival of axotomized retinal ganglion cells in adult mammals. Clin Neurosci. 1997;4:233–39.
43. Nizari S, Guo L, Davis BM, Normando EM, Galvao J, Turner LA, Bizrah M, Dehabadi M, Tian K, Francesca Cordeiro M. Non-amyloidogenic effects of alpha2 adrenergic agonists: implications for brimonidine-mediated neuroprotection. Cell Death Dis. 2016;7(12):e2514. doi:10.1038/cddis.2016.397.
44. Yan P, Tang S, Zhang H, Guo Y, Zeng Z, Wen Q. Palmitic acid triggers cell apoptosis in RGC-5 retinal ganglion cells through the Akt/FoxO1 signaling pathway. Metab Brain Dis. 2016;32:453–60.
45. Hu Y. Axon injury induced endoplasmic reticulum stress and neurodegeneration. Neural Regen Res. 2016;11(10):1557–59. doi:10.4103/1673-5374.193225.

46. Yi J, Puyang Z, Feng L, Duan L, Liang P, Backman V, Liu X, Zhang HF. Optical detection of early damage in retinal ganglion cells in a mouse model of partial optic nerve crush injury. Invest Ophthalmol Vis Sci. 2016;57(13):5665–71. doi:10.1167/iovs.16-19955.
47. Zhang SH, Gao FJ, Sun ZM, Xu P, Chen JY, Sun XH, Wu JH. High pressure-induced mtDNA alterations in retinal ganglion cells and subsequent apoptosis. Front Cell Neurosci. 2016;10:254. doi:10.3389/fncel.2016.00254.
48. Cai W, Rudolph JL, Harrison SM, Jin L, Frantz AL, Harrison DA, Andres DA. An evolutionarily conserved Rit GTPase-p38 MAPK signaling pathway mediates oxidative stress resistance. Mol Biol Cell. 2011;22(17):3231–41. doi:10.1091/mbc.e11-05-0400.